The neutron diffraction study of pyridinium periodate at 352, 300 and 100 K

2003 J. Phys.: Condens. Matter 15 5663

(http://iopscience.iop.org/0953-8984/15/33/301)

INSTITUTE OF PHYSICS PUBLISHING JOURNAL OF PHYSICS: CONDENSED MATTER

J. Phys.: Condens. Matter **15** (2003) 5663–5674 PII: S0953-8984(03)63084-5

The neutron diffraction study of pyridinium periodate at 352, 300 and 100 K

Hanna Małuszyńska[1], Christian Scherf[2,3], Piotr Czarnecki[1] and Alain Cousson[3]

[1] Faculty of Physics, A Mickiewicz University, Umultowska 85, 61-614 Poznań, Poland
[2] Institut für Kristallographie, RWTH Aachen, 52056 Aachen, Germany
[3] Laboratoire Léon Brillouin (CEA-CNRS), CEA Saclay, 91191 Gif-sur-Yvette Cedex, France

Received 1 May 2003
Published 8 August 2003
Online at stacks.iop.org/JPhysCM/15/5663

Abstract

The crystal and molecular structure of pyridinium periodate $[H_5C_5NH]^+[IO_4]^-$ (hereafter referred to as $PyIO_4$) was re-determined by single-crystal neutron diffraction at 350, 300 and 100 K. The structures of the high-temperature paraelectric and the ferroelectric intermediate phase confirmed the x-ray results. The low-temperature ferroelectric phase at 100 K, for which x-ray results did not agree with dielectric measurements, was uniquely determined by neutron diffraction. The sequence of space groups and continuous phase transitions is $Cmcm(\mathrm{I}) \xrightarrow{321\ \mathrm{K}} Cmc2_1(\mathrm{II}) \xrightarrow{210\ \mathrm{K}} C112_1(\mathrm{III})$. The structure of the low-temperature phase III is consistent with all physical measurements. The continuous phase transition at $T_2 = 210$ K is not just accompanied by symmetry lowering but also by reversible twinning by pseudo-merohedry. The dipole moment of the ions of the low ferroelectric phase was calculated using the Gaussian 98 program. The theoretical value agrees well with the experimental spontaneous polarization measurements from the pyroelectric effect. The $PyIO_4$ belongs to the order–disorder class of ferroelectrics.

1. Introduction

The pyridinium periodate, $[H_5C_5NH]^+[IO_4]^-$ (hereafter $PyIO_4$) belongs to a large family of molecular ionic salts in which the organic cations and/or the anions reveal positional order but orientational disorder. The molecular dynamics of the pyridinium cations of these salts evidently appear to be related to the existing polymorphic solid–solid phase transitions [1–3].

In the pyridinium salts the transformation from disordered to ordered phase occurs by one, two or three solid–solid phase transitions. Recently we discovered that, in pyridinium salts with tetrahedral anions such as BF_4 [4], ClO_4 [2], ReO_4 [3], IO_4 [5], FSO_3 [6], $FCrO_3$ [7], there are at least two solid–solid phase transitions and the intermediate and sometimes low-temperature phases reveal ferroelectric properties. The phase transition from the disordered

high-temperature phase to the ferroelectric phase is of order–disorder type [2–4, 8]. However, the NMR [3–7], muon [9] and dielectric spectroscopy [5, 10] measurements indicate that, in the intermediate ferroelectric phase, there are still reorientations of pyridinium cations. This indicates that this phase should be considered to be disordered, like the high-temperature phase. The appearance of ferroelectric properties at the phase transition is caused by the change in reorientation of pyridinium cations in such a way that the pyridinium dipoles create an average non-zero component along the ferroelectric axis. The additional deformation of tetrahedral anions may also contribute to the total spontaneous polarization. The precise determination of crystal and molecular structure is essential for explaining the nature of the ferroelectric properties of pyridinium salts.

Pyridinium periodate is of special interest because its Curie temperature, $T_1 = 321$ K, is above room temperature [5]. The second non-ferroelectric phase transition occurs at temperature $T_2 = 210$ K and appears to be continuous. In the previous paper [11] the crystal and molecular structure of $PyIO_4$ was determined by x-ray diffraction at 350, 300 and 100 K. The high-temperature and intermediate phases are orthorhombic, while the low-temperature phase is monoclinic with the phase transition sequence $Cmcm(\mathrm{I}) \xrightarrow{321\ \mathrm{K}} Cmc2_1(\mathrm{II}) \xrightarrow{210\ \mathrm{K}} C2(\mathrm{III})$. Phase I at 350 K and phase II at 300 K are partially disordered, while the low-temperature phase is positionally and orientationally well ordered.

However, the symmetry of phase III, obtained from x-ray data, is controversial. For the symmetry transformation from $Cmc2_1$ to $C2$ the vector of spontaneous polarization would have been turned by 90° from the z-axis of orthorhombic $mm2$ to the y-axis of monoclinic 2 symmetry, contradicting the results from measurements of the dielectric and pyroelectric effects on monocrystals [12].

The determination of x-ray structure is biased by a high absorption. This concerns not only the symmetry and space group of phase III but also the precise bond lengths and angles and occupancy parameters of the carbon and nitrogen atoms of the pyridinium cation in all three phases. These accurate values are crucial for an explanation of the origin of the ferrolectricity in this compound and could be obtained only from the neutron diffraction data.

In this paper we present results of accurate structural investigations by neutron diffraction of all three phases. We also show the results of neutron diffraction at room temperature after cooling and heating. This proves that all phase transitions are reversible, apart from the many irreversible defects and cracks inside the crystal that appear during the phase transition $\mathrm{II} \xrightarrow{321\ \mathrm{K}} \mathrm{I}$. The important extinction effect observed during the first room-temperature data collection decreased slightly in the low-temperature phase III and vanished completely during the high-temperature and the final room-temperature data collection experiments.

For the first time we report a precise molecular structure of an ordered pyridinium cation at 100 K, allowing us to calculate a dipole moment of the pyridinium cation by using the Gaussian 98 program. We have calculated the spontaneous polarization from the theoretical dipole moments and compared it with the experimentally determined value from the pyroelectric effect. The refinement of the pyridinium cation N atom occupancy factor in the disordered ferroelectric II phases allowed us to establish a more precise model of ferroelectricity in this compound.

2. Experimental details

Neutron diffraction experiments were carried out on the P110 single-crystal diffractometer located on the hot source of the ORPHEE reactor at the LLB in Saclay, France. The wavelength used ($\lambda = 0.8350$ Å) was selected by a horizontally focusing Cu(220) monochromator and the harmonic $\lambda/2$ contamination was attenuated to 10^{-3} by an erbium filter. All reflections

Table 1. Crystal data and neutron structure refinement for pyridinium periodate $[C_5H_5NH]^+[IO_4]^-$ at 352, 300†, 100 and 300‡ K. We used an as-grown crystal at 300† K and the same crystal at 300‡ K after cooling to 150 K, heating to 352 K and cooling again to 300 K. (Note: For the definition of R_1, ωR_2 and other values presented in table 1, see the manual for SHELXL-97 [15].)

Temperature (K)	352	300†	100	300‡
Formula weight		$[C_5H_5NH]^+[IO_4]^-$		
Crystal system	Orthorhombic	Orthorhombic	Monoclinic	Orthorhombic
Space group	$Cmcm$	$Cmc2_1$	$C112_1$	$Cmc2_1$
Unit cell dimension (Å)	8.398(18)	8.369(18)	8.25(3)	8.36(2)
	7.348(16)	7.29(2)	7.11(2)	7.28(2)
	12.76(4)	12.73(4)	12.80(2)	12.76(4)
			$\gamma = 90.5(2)$	
Number of reflections used for unit cell dimension	36	22	36	14
Volume (Å^3)	788(4)	777(4)	751(3)	777(4)
Z	4	4	4	4
Density (calculated) (mg m^{-3})	2.632	2.668	2.742	2.668
Absorption coefficient (cm^{-1})		1.075		
Crystal size (mm)		$4 \times 4 \times 5$		
Theta range (degrees)	3.76–37.59	3.7–42.48	1.87–42.72	3.76–42.50
Reflections collected	1548	1337	2322	1837
Unique, R (int)	685, 0.0890	954, 0.0394	1726, 0.0381	1137, 0.0440
Refinement method		Full-matrix least squares on F^2		
Data/restraints/parameters	685/4/50	954/6/89	1726/1/156	1137/6/89
Goodness of fit on F^2	1.314	1.765	1.651	1.237
R indices $[I > 2\sigma(I)]$:				
R_1	0.0528	0.0567	0.0269	0.0396
ωR_2	0.0867	0.0793	0.0549	0.0521
R indices (all data):				
R_1	0.1155	0.1039	0.0277	0.0836
ωR_2	0.0954	0.0847	0.0550	0.0562
Extinction coefficient	0.0019(19)	0.147(7)	0.0206(14)	0.0029(8)
Largest difference, peak and hole (e Å^{-3})	0.332, −0.417	0.494, −0.465	0.691, −1.025	0.524, −0.414

were measured using the ω-scan technique. At low and high temperatures we used an Oxford Instruments liquid helium evaporation cryostat and a special furnace adapted to the diffractometer, respectively.

Four data-sets were collected at 300, 100, 352 and (again) 300 K. The temperatures were maintained within ±1 K. The crystal, in an envelope of aluminium foil, was glued with its c-axis parallel to the ϕ-axis of the Eulerian cradle and with its ψ-angle equal to zero for all temperatures. This set-up was required to collect all diffracted intensities, even of the split reflections of phase III at 100 K. No significant intensity variations were observed for two standard reflections. Their standard deviations were used to calculate the McCandlish factor [13].

Data reduction was carried out using PRON2K[4]. Our large single crystal (with a sample volume of about 80 mm^3) with an experimentally determined absorption coefficient of $\mu = 1.075$ mm^{-1} at $\lambda = 0.8350$ Å required the application of analytical absorption correction using the DATAP program[5]. The absorption corrections were applied to all data-sets except at

[4] PRON2K, DATA REDUCTION FOR STOE 'DIF4', version for Institut für Kristallographie, RWTH Aachen.
[5] DATAP, July 1987 version, Institut Laue-Langevin.

Table 2. Atomic coordinates ($\times 10^4$) and equivalent isotropic displacement parameters ($\times 10^3$ Å^2) for $PyIO_4$ at (a) 352, (b) 300†, (c) 100 and (d) 300‡ K. U(eq) is defined as one third of the trace of the orthogonalized U_{ij}-tensor; OF is an occupancy factor.

	x	y	z	U_{eq}	OF
			(a) $T = 352$ K		
I(1)	0	6435(3)	2500	52(1)	0.25
O(1)	0	5104(5)	1368(2)	113(1)	0.50
O(2)	1717(3)	7776(3)	2500	101(1)	0.50
C(1)/N	1619(2)	0	5000	76(1)	0.468/0.031(2)
C(2)/N	819(1)	1008(1)	4282(1)	75(1)	0.781/0.219(1)
H(1)	2891(4)	0	5000	140(2)	0.50
H(2)	1429(5)	1792(5)	3705(2)	127(2)	1.0
			(b) $T = 300^\dagger$ K		
I(1)	0	1468(2)	4980(3)	35(1)	0.50
O(1)	−1723(3)	2823(3)	5101(2)	73(1)	1.0
O(2)	0	−129(6)	6014(4)	71(1)	0.50
O(3)	0	400(9)	3758(3)	76(1)	0.50
C(1)/N	−821(4)	5978(3)	3173(1)	54(1)	0.914/0.086(2)
C(2)/N	−1637(1)	4931(4)	2444(3)	51(1)	0.931/0.069(3)
C(3)/N	−820(3)	3936(2)	1737(1)	45(1)	0.655/0.345(3)
H(1)	−1462(11)	6789(10)	3740(5)	90(2)	1.0
H(2)	−2913(3)	4911(12)	2383(9)	93(2)	1.0
H(3)	−1415(10)	3136(10)	1160(4)	89(2)	1.0
			(c) $T = 100$ K		
I(1)	−106(2)	1566(1)	4995(1)	9(1)	1.0
O(1)	−1966(2)	2806(2)	5174(1)	14(1)	1.0
O(2)	64(2)	−106(2)	6013(3)	18(1)	1.0
O(3)	−90(2)	487(2)	3748(1)	20(1)	1.0
O(4)	1542(2)	3138(1)	5083(1)	16(1)	1.0
N(1)	−893(1)	3850(1)	1739(1)	13(1)	1.0
C(2)	733(1)	3889(2)	1728(1)	14(1)	1.0
C(3)	1548(1)	4951(2)	2460(1)	14(1)	1.0
C(4)	656(1)	5975(2)	3195(1)	14(1)	1.0
C(5)	−1034(1)	5919(2)	3179(1)	14(1)	1.0
C(6)	−1792(1)	4827(2)	2432(1)	14(1)	1.0
H(1)	−1491(4)	3064(5)	1176(3)	30(1)	1.0
H(2)	1344(4)	3054(5)	1128(3)	33(1)	1.0
H(3)	2869(3)	4975(5)	2456(4)	34(1)	1.0
H(4)	1268(4)	6832(5)	3780(3)	33(1)	1.0
H(5)	−1759(4)	6716(5)	3732(3)	33(1)	1.0
H(6)	−3104(3)	4720(5)	2360(3)	33(1)	1.0
			(d) $T = 300^\ddagger$ K		
I(1)	0	1470(2)	4988(2)	37(1)	0.50
O(1)	−1723(2)	2829(2)	5101(2)	76(1)	1.0
O(2)	0	−124(4)	6011(3)	70(1)	0.50
O(3)	0	406(5)	3759(2)	80(1)	0.50

Table 2. (Continued.)

	x	*y*	*z*	U_{eq}	OF
C(1)/N	−819(3)	5980(2)	3173(1)	56(1)	0.932/0.068(2)
C(2)/N	−1633(1)	4941(3)	2444(2)	54(1)	0.944/0.056(2)
C(3)/N	−813(2)	3942(2)	1737(1)	49(1)	0.624/0.376(2)
H(1)	−1461(8)	6791(8)	3743(3)	99(2)	1.0
H(2)	−2916(3)	4909(9)	2407(8)	99(1)	1.0
H(3)	−1415(8)	3146(7)	1165(3)	91(1)	1.0

100 K, where the final results were significantly better without correction. The reason may be an anisotropic extinction behaviour in phase III originating from the domain structure of the pseudo-merohedral twins with complementary effects to the absorption. The structures were solved and refined using SHELXS [14] and SHELXL-97 [15], respectively.

A summary of crystal data and the computational details are presented in table 1. Atomic coordinates and equivalent temperature factors at 352, 300†, 100 and 300‡ K are given in table 2, and bond lengths and angles in table 3. The experiment was performed at 300† K with an as-grown crystal and at 300‡ K after cooling, heating and cooling again to 300 K.

The spontaneous polarization was obtained from the pyroelectric effect measurements carried out using a Keithley 6514 electrometer along the ferroelectric axis [001]. An x-ray oriented sample of 0.3 mm in thickness and 10 mm^2 in area was used. The crystal was cooled at a rate of 2 K min^{-1} in an electric field of 2 kV cm^{-1} down to 120 K to obtain a single domain state and then measurements of the pyroelectric effect were performed during heating at a rate of 1.5 K min^{-1}.

3. Results and discussion

The neutron results confirmed the structure of the high-temperature phase (I) at 352 K and the intermediate phase (II) at 300 K (which were determined by x-ray diffraction [11]) and uniquely determined the structure of low-temperature phase (III) at 100 K. The phase transition sequence of $PyIO_4$ is $Cmcm$(I) → $Cmc2_1$(II) → $C112_1$(III). The non-standard monoclinic space group setting was selected to maintain the same crystal lattice directions in all three phases. It can be transformed to the standard $P2_1$ setting with half-cell volume by applying the transformation matrix $\left(\frac{1}{2}\ \frac{1}{2}\ 0,\quad 0\ 0\ -1,\quad -\frac{1}{2}\ \frac{1}{2}\ 0\right)$. Although the final *R*-values of the neutron refinements for the phases (I) and (II) do not differ significantly from their x-ray equivalents, the neutron results allow us to describe the dynamic pyridinium cation disorder with significantly higher precision.

In phase I at 352 K the pyridinium cation is on a $2/m$ site with one carbon atom C(1) on the twofold axis 2 and C(2) in a general position. Unlike the x-ray data, the neutron data refinement of the average N atom occupancy factors results in significant values: 6.3(2)% of the N atom at C(1) and 21.9(1)% at C(2) sites. (For our x-ray data of phase I, their equivalents could not be resolved and they were simply fixed to equal the nitrogen distribution on all six possible positions, i.e. 83.3% carbon and 16.7% nitrogen site occupancy [11].)

In the intermediate ferroelectric phase II at 300 K the pyridinium cation is at an *m* site and the N distribution is even more localized: there is 8.6(3)% average occupation probability for the N atom at C(1), 6.9(3)% at C(2), and 34.5(3)% at C(3) sites. It is worth noticing that the largest part of an average N atom occupancy factor in disordered phases I and II is at the same site, which is fully occupied by an N atom in the low-temperature phase III.

Table 3. Bond lengths (Å) and valence angles (degrees) in $PyIO_4$ at (a) 352, (b) 300† and 100 K.

Bond length (Å)		Bond angles (degrees)	
		(a) $T = 352$ K	
I–O(1)	1.744(6)	O(1)–I–O(2)	108.4(2)
I–O(2)	1.747(5)	O(1)–I–O(1)[b]	111.8(3)
		O(2)–I–O(2)[a]	111.0(3)
C(1)–C(2)	1.357(4)	C(2)–C(1)–C(2)[c]	120.6(2)
C(1)–H(1)	1.068(4)	C(2)–C(1)–H(1)	119.7(2)
C(2)–C(2)[d]	1.357(4)	C(2)[c]–C(1)–H(1)	119.7(2)
C(2)–H(2)	1.066(5)	C(1)–C(2)–C(2)[c]	119.7(2)
		C(1)–C(2)–H(2)	121.6(3)
		C(2)[d]–C(2)–H(2)	118.7(3)
		(b) $T = 300^{\dagger}$ K	
I–O(1)	1.755(5)	O(1)–I–O(2)	107.9(3)
I–O(2)	1.757(5)	O(1)–I–O(3)	109.3(3)
I–O(3)	1.741(8)	O(1)–I–O(1)[d]	110.5(3)
		O(2)–I–O(3)	111.9(4)
C(1)–C(2)	1.382(6)	C(2)–C(1)–C(1)[d]	119.6(2)
C(1)–C(1)[d]	1.374(7)	C(2)–C(1)–H)1)	120.5(6)
C(2)–C(3)	1.343(5)	C(1)[d]–C(1)–H(1)	119.9(6)
C(3)–C(3)[d]	1.372(5)	C(1)–C(2)–C(3)	119.8(2)
C(1)–H(1)	1.076(7)	C(1)–C(2)–H(2)	123.3(6)
C(2)–H(2)	1.071(4)	C(3)–C(2)–H(2)	116.8(5)
C(3)–H(3)	1.062(6)	C(2)–C(3)–C(3)[d]	120.6(2)
		C(2)–C(3)–H(3)	121.4(6)
		C(3)[d]–C(3)–H(3)	118.0(5)
		(c) $T = 100$ K	
I(1)–O(1)	1.791(6)	O(1)–I(1)–O(2)	108.1(2)
I(1)–O(2)	1.770(4)	O(1)–I(1)–O(3)	109.7(2)
I(1)–O(3)	1.772(4)	O(1)–I(1)–O(4)	109.9(2)
I(1)–O(4)	1.756(6)	O(2)–I(1)–O(3)	111.8(2)
		O(2)–I(1)–O(4)	108.4(2)
		O(3)–I(1)–O(4)	109.0(2)
N(1)–C(2)	1.341(4)	C(2)–N(1)–C(6)	123.3(2)
N(1)–C(6)	1.352(4)	C(2)–N(1)–H(1)	118.4(3)
		C(6)–N(1)–H(1)	118.3(3)
		N(1)–C(2)–C(3)	119.2(2)
		N(1)–C(2)–H(2)	117.1(3)
		C(3)–C(2)–H(2)	123.4(3)
		C(2)–C(3)–C(4)	119.1(2)
		C(2)–C(3)–H(3)	119.5(3)
		C(4)–C(3)–H(3)	121.4(3)
		C(3)–C(4)–C(5)	120.1(2)
		C(3)–C(4)–H(4)	120.7(3)
		C(5)–C(4)–H(4)	119.3(3)
		C(4)–C(5)–C(6)	118.6(2)
		C(4)–C(5)–H(5)	121.7(3)
		C(6)–C(5)–H(5)	119.7(3)
		N(1)–C(6)–C(5)	119.8(2)
		N(1)–C(6)–H(6)	117.0(3)
		C(5)–C(6)–H(6)	123.2(3)

Table 3. (Continued.)

Bond length (Å)		Bond angles (degrees)	
C(2)–C(3)	1.375(4)	N(1)–C(2)–H(2)	117.4(3)
C(3)–C(4)	1.402(4)	C(3)–C(2)–H(2)	123.4(3)
C(4)–C(5)	1.394(4)	C(2)–C(3)–C(4)	119.1(2)
C(5)–C(6)	1.378(4)	C(2)–C(3)–H(3)	119.3(3)
N(1)–H(1)	1.034(4)	C(4)–C(3)–H(3)	121.6(3)
C(2)–H(2)	1.097(4)	C(3)–C(4)–C(5)	120.3(2)
C(3)–H(3)	1.090(4)	C(3)–C(4)–H(4)	120.7(3)
C(4)–H(4)	1.087(4)	C(5)–C(4)–H(4)	119.0(3)
C(5)–H(5)	1.089(4)	C(4)–C(5)–C(6)	118.4(2)
C(6)–H(6)	1.088(4)	C(4)–C(5)–H(5)	122.0(3)
		C(6)–C(5)–H(5)	119.7(3)
		N(1)–C(6)–C(5)	119.8(2)
		N(1)–C(6)–H(6)	117.2(3)
		C(5)–C(6)–H(6)	123.0(3)

[a] $-x.y, -z + 1/2$.
[b] $x, y, -z + 1/2$.
[c] $x, -y, -z + 1$.
[d] $-x, y, z$.

The results discussed above are crucial to the interpretation of the molecular dynamics of pyridinium cations obtained from NMR data. Until now we interpreted the dynamics of the pyridinium cation as reorientations among equivalent energy barriers around a pseudo-sixfold axis perpendicular to the cation plane in the paraelectric high-temperature phase (I) and as reorientations among inequivalent energy barriers in the ferroelectric intermediate phase (II). These results confirmed the existence of inequivalent barriers in both (I) and (II) phases and allow for quantitative interpretation of the pyridinium dynamics.

In the high-temperature phase (I) and the room-temperature phase (II) the IO_4 anions are well ordered. In phase I the IO_4 ion is at an $m2m$ site while in the ferroelectric phase II is at an m site. The mean I–O bond lengths are 1.745(5) Å in phase I and 1.751(6) Å in phase II, with O–I–O angles that vary from 108.4° to 111.8° and 107.9(3)° to 111.9(4)° in phases I and II, respectively. While in phase I the two symmetry-independent C–C bonds are equal to 1.357(4) Å, the non-equal distribution of the N atom in phase II gives rise to one shorter C(2)–N/C(3) bond of 1.343(5) Å and three longer bonds that range from 1.372(5) to 1.382(6) Å C–C bond lengths.

The low-temperature phase (III) at 100 K is monoclinic (space group $C112_1$) with γ angle = 90.5°. The mirror plane perpendicular to the a-axis and the c-glide perpendicular to the y-axis that are present in phase II vanish, so the only remaining symmetry element apart from c-centring is the polar 2_1 axis parallel to z. The monoclinic $C112_1$ space group is consistent with dielectric measurements, which indicates that the spontaneous polarization vector remains parallel to the z-axis at the 210 K phase transition [12].

The $T_2 = 210$ K continuous phase transition with the change of crystal system and space group is accompanied by reversible pseudo-merohedral twinning [16]. The twin operator $\left(-1\,0\,0,\quad 0\,1\,0,\quad 0\,0\,1\right)$, which belongs to the former higher symmetric space group of phase II and was introduced in the last cycles of the refinement, significantly lowered the R value from 10.78 to 2.74%. The corresponding twin law is the mirror plane perpendicular to the a-axis. The small deviation from the exact 90° γ angle causes the formation of two ferroelastic domain states with approximately $\frac{1}{3}$ and $\frac{2}{3}$ volume fractions. The SHELXL BASF

Table 4. The hydrogen bonds in $PyIO_4$ in phase I at 352 K, phase II at 300† K and phase III at 100 K.

Donor	Acceptor	H···O (Å)	D···A (Å)	< D–HO (degrees)	Symmetry operation
			$T = 352$ K		
C(1)–H(1)	O(1)	2.488(8)	3.334(9)	135.4(2)	$-x+\frac{1}{2}, -y+\frac{1}{2}, z+\frac{1}{2}$
C(2)–H(2)	O(2)	2.304(7)	3.338(9)	162.7(4)	$-x+\frac{1}{2}, y-\frac{1}{2}, -z+\frac{1}{2}$
			$T = 300$ K		
C(1)–H(1)	O(1)	2.42(1)	3.472(10)	153.2(4)	$-x-\frac{1}{2}, y+\frac{1}{2}, z$
C(2)–H(2)	O(2)	2.47(1)	3.356(9)	139.0(8)	$-x-\frac{1}{2}, -y+\frac{1}{2}, z-\frac{1}{2}$
C(2)–H(2)	O(3)	2.50(1)	3.292(9)	130.1(1)	$-\frac{1}{2}+x, \frac{1}{2}+y, z$
C(3)–H(3)	O(1)	2.176(9)	3.196(2)	160.2(7)	$-x-\frac{1}{2}, -y+\frac{1}{2}, z-\frac{1}{2}$
C(3)–H(3)	O(2)	2.50(1)	3.004(10)	108.1(6)	$-x, -y, z-\frac{1}{2}$
			$T = 100$ K		
N(1)–H(1)	O(1)	1.907(6)	2.913(8)	163.3(3)	$-x-\frac{1}{2}, -y+\frac{1}{2}, z-\frac{1}{2}$
N(1)–H(1)	O(2)	2.428(8)	2.907(8)	107.2(3)	$-x, -y, z-\frac{1}{2}$
C(2)–H(2)	O(2)	2.392(8)	2.912(8)	107.2(3)	$-x, -y, z-\frac{1}{2}$
C(2)–H(2)	O(4)	2.361(7)	3.409(9)	159.3(3)	$-x+\frac{1}{2}, -y+\frac{1}{2}, z-\frac{1}{2}$
C(3)–H(3)	O(3)	2.385(7)	3.245(9)	134.7(4)	$x+\frac{1}{2}, y+\frac{1}{2}, z$
C(4)–H(4)	O(1)	2.401(7)	3.451(9)	162.0(3)	$x+\frac{1}{2}, y+\frac{1}{2}, z$
C(5)–H(5)	O(4)	2.451(7)	3.534(9)	172.9(3)	$x-\frac{1}{2}, y+\frac{1}{2}, z$
C(6)–H(6)	O(3)	2.480(7)	3.236(9)	125.6(3)	$x-\frac{1}{2}, y+\frac{1}{2}, z$
C(6)–H(6)	O(2)	2.381(7)	3.260(9)	136.8(3)	$-x-\frac{1}{2}, -y+\frac{1}{2}, z-\frac{1}{2}$

parameter converged to 0.329(2). All hkl reflections with $h \neq 0$ are split with an angle that depends on the h contribution of the reflection index, i.e. $h00$ reflections show the most important splitting and $0kl$ reflections are not split at all.

The low-temperature phase of $PyIO_4$ is fully ordered, with one pyridinium cation and one IO_4 anion in the smallest $P2_1$ asymmetric unit. There are no symmetry-related atoms in either ion. In the IO_4 anion the I–O(1) bond is significantly longer than the three remaining I–O bonds due to the presence of the N–H···O(1) hydrogen bond. The O–I–O angles range from 108.1(2)° to 111.8(2)°, with a mean value of 109.5(2)°. All bond lengths and angles in pyridinium agree well with the expected values (the mean $N^{+}_{sp^2}$–C_{sp^2} of 1.346(4) Å and mean C_{sp^2}–C_{sp^2} of 1.387(4) Å).

The basic crystal structure network (figures 1 and 2) based on pyridinium cations that are hydrogen-bonded to isolated tetrahedral IO_4 anions is almost identical in all three phases. The C/N–H···O hydrogen bond geometries are given in table 4. The H···O distances and the C/N–H···O angles in the high-temperature phase (I) and the room-temperature phase (II) with disordered pyridinium cations confirm the correct refinement of the nitrogen occupancy factors, because the H···O distances are significantly shorter and the C/N–H···O angles are larger when the nitrogen atom is either entirely or partly involved in hydrogen bonds (as in either phase III or phases I and II, respectively).

The origin of ferroelectricity in $PyIO_4$ may be related to the ordering of the dipole moments of both ions and/or to the displacement of the two ionic sublattices. The pyridinium cation is non-centrosymmetric and carries a dipole moment. However, in the centrosymmetric paraelectric phase I, the disordered pyridinium cation is at $2/m$ site symmetry and its averaged dipole moment is equal to zero. The site symmetry of the IO_4 anion is $m2m$ and its geometry

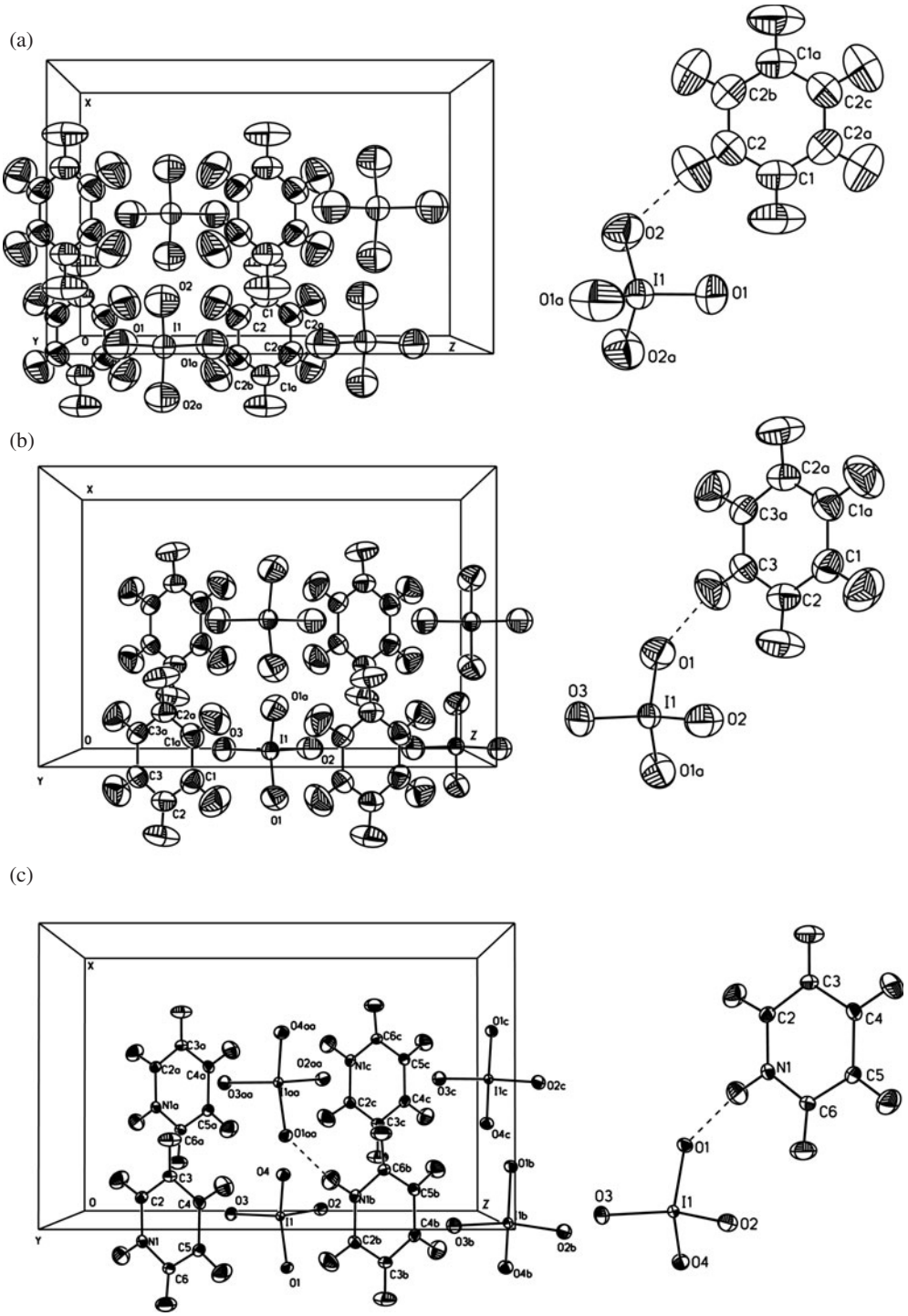

Figure 1. The packing arrangement in three phases at (a) 352, (b) 300 and (c) 100 K down the *y*-axis. On the right are the corresponding ORTEP drawings at 50% probability.

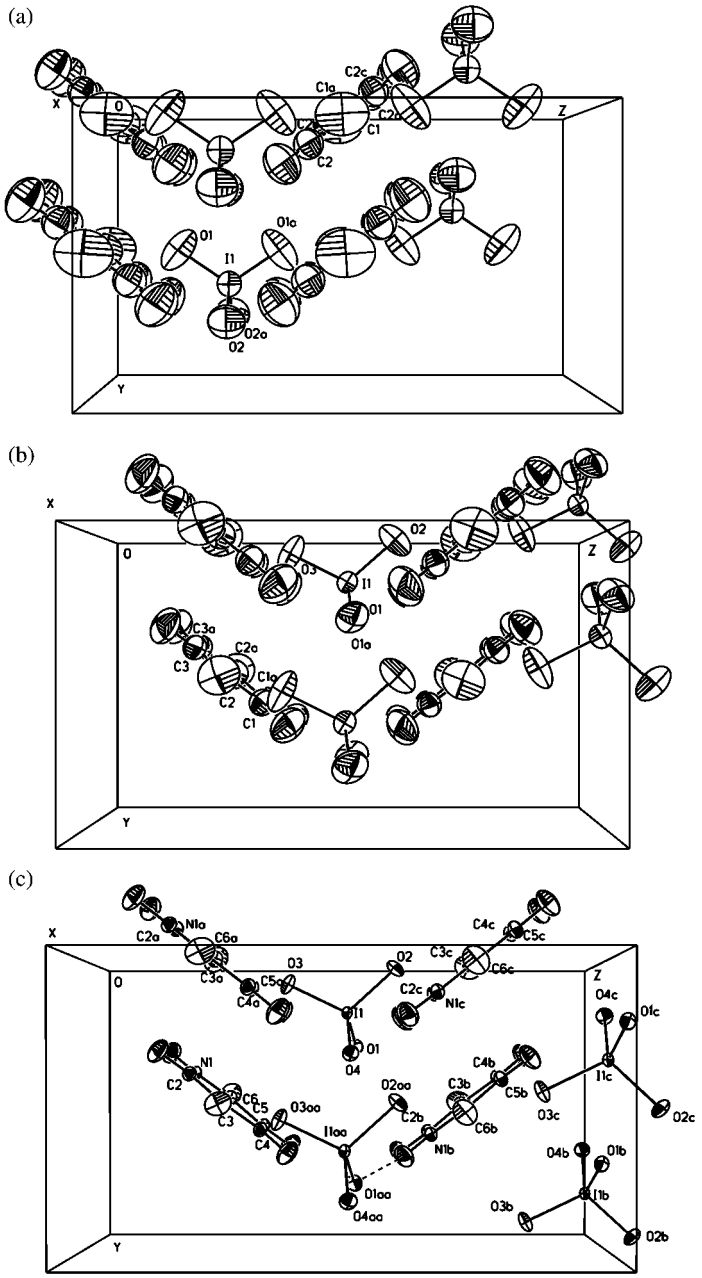

Figure 2. The packing arrangement in three phases at (a) 350, (b) 300 and (c) 100 K down the *x*-axis.

is slightly distorted from a regular tetrahedron, which also creates a small dipole moment for this originally non-polar ion. Nevertheless, the total averaged dipole moment of all four anions in the centrosymmetric unit cell will add to zero. Below the ferroelectric Curie point ($T_1 = 322$ K) one symmetry plane disappears, resulting in a non-zero average dipole moment of both ions for phase II. The disorder of both ions decreases with decreasing temperature.

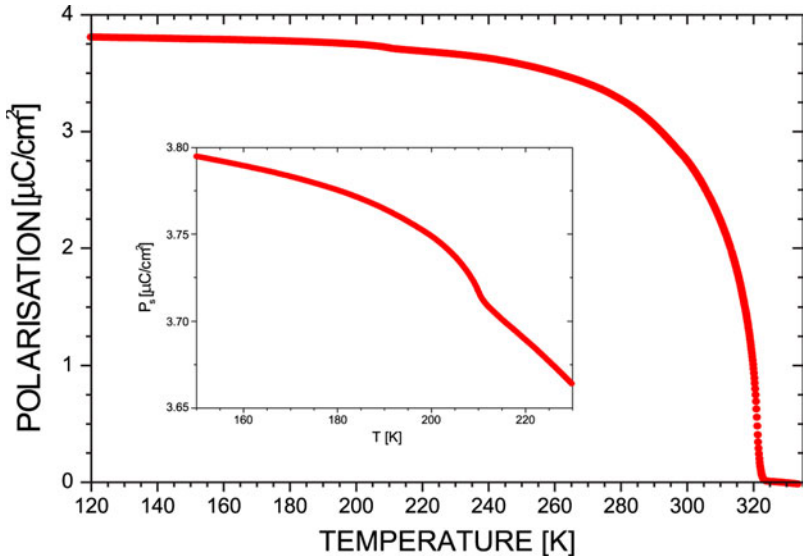

Figure 3. Temperature dependence of spontaneous polarization from pyroelectric measurements. The spontaneous polarization dependence on temperature in the vicinity of T_2 is shown in the inset. (This figure is in colour only in the electronic version)

The results of the spontaneous polarization measurements using the pyroelectric effect are presented in figure 3. The spontaneous polarization reaches about 3.3 μC cm^{-2} at 120 K and disappears at the Curie point. In the inset of figure 3 one can see a small anomaly in the spontaneous polarization in the vicinity of T_2, which confirms the continuous character of the phase transition from phase II to phase III [7, 11].

The change in the spontaneous polarization with temperature (figure 3) can be explained qualitatively by the change in the nitrogen atom occupancy factor. In the vicinity of the ferroelectric phase transition temperature T_1 there should be a continuous change in the cation disorder and the nitrogen occupancy factor, leading to the final change in the cation site symmetry from m to $2/m$ and the disappearance of the average dipole moment of the cation above T_1.

In order to compare the theoretical and the experimental values of spontaneous polarization that were obtained from the pyroelectric measurements, we have calculated the dipole moments with the ion geometry of the well ordered low-temperature phase at 100 K with Gaussian 98 using the simple 6-51G* basis set. The calculated pyridinium dipole moment is 1.97 D and points towards the nitrogen atom. Its component along the polar z-axis is about 1.55 D. Taking into account only this pyridinium contribution to the calculation, we obtain a spontaneous polarization of about 2.9 μC cm^{-2}, a value that is still lower than the experimental spontaneous polarization that was measured according to figure 3. The calculated IO_4 anion dipole moment is about 0.27 D and points towards the same direction along the polar axis as the pyridinium cation dipole moment. Consequently, both ions contribute to the summarized spontaneous polarization in the low-temperature ordered phase. The total calculated spontaneous polarization without a displacement component is about 3.2 μC cm^{-2}, which is in good agreement with the measured value of 3.3 μC cm^{-2}.

Therefore we conclude that the displacement component of the spontaneous polarization is negligible. So, we can classify $PyIO_4$ as an order–disorder type ferroelectric.

Acknowledgments

The experiments at LLB were supported by the European Commission through the Access to Research Infrastructures action of the Improving Human Potential Programme (contract no HPRI-CT-1999-00032). We wish to thank Dr Anna Czarnecka for growing the monocrystals of $PyIO_4$.

References

[1] Ripmeester J A 1986 *J. Chem. Phys.* **85** 747
[2] Czarnecki P, Nawrocik W, Pająk Z and Wąsicki J 1994 *J. Phys.: Condens. Matter* **6** 4955
[3] Wąsicki J, Czarnecki P, Pająk Z, Nawrocik W and Szczepański W 1997 *J. Chem. Phys.* **107** 576
[4] Czarnecki P, Nawrocik W, Pająk Z and Wąsicki J 1994 *Phys. Rev.* B **49** 1511
[5] Pająk Z, Czarnecki P, Wąsicki J and Nawrocik W 1998 *J. Chem. Phys.* **109** 6420
[6] Pająk Z, Czarnecki P, Małuszyńska H, Szafrańska B and Szafran M 2000 *J. Chem. Phys.* **113** 848
[7] Pająk Z, Małuszyńska H, Szafrańska B and Czarnecki P 2002 *J. Chem. Phys.* **117** 5303
[8] Czarnecki P, Katrusiak A, Szafraniak I and Wąsicki J 1998 *Phys. Rev.* B **57** 3326
[9] Beck B, Roduner E, Dilger H, Czarnecki P, Fleming D G, Reid I D and Rhodes C J 2000 *Physica* B **289–290** 607
[10] Czarnecki P and Szafraniak I 1998 *Phys. Status Solidi* b **209** 211
[11] Maluszynska H, Czarnecki P, Lewicki S, Wasicki J and Gdaniec M 2001 *J. Phys.: Condens. Matter* **13** 11053
[12] Czapla Z, Dacko S and Kosturek B 2000 *Z. Naturf.* a **55** 891
[13] McCandlish L E, Stout G H and Andrews L C 1975 *Acta Crystallogr.* A **31** 245–9
[14] Sheldrick G 1997 *SHELXS-97 Program for Crystal Structure Determination* University of Goettingen
[15] Sheldrick G 1997 *SHELXL-97 Program for Crystal Structure Determination* University of Goettingen
[16] Herbst-Irmer R and Sheldrick G 1998 *Acta Crystallogr.* B **54** 443–9